Ultrafast polymer dynamics through a nanopore

Journal:	*Nano Letters*
Manuscript ID	Draft
Manuscript Type:	Communication
Date Submitted by the Author:	n/a
Complete List of Authors:	Lin, Chih-Yuan; University of Pennsylvania, Physics and Astronomy Fotis, Riley ; University of Pennsylvania, Physics and Astronomy Xia , Zehui; Goeppert, LLC Kavetsky, Kyril ; University of Pennsylvania, Physics and Astronomy; University of Pennsylvania, Materials Science and Engineering Chou, Yung-Chien ; University of Pennsylvania, Physics and Astronomy Niedzwiecki, David; Goeppert LLC Biondi, Michele; ELEMENTS SRL Thei, Federico; ELEMENTS SRL Drndić, Marija; University of Pennsylvania, Physics and Astronomy

Ultrafast polymer dynamics through a nanopore

Chih-Yuan Lin[1#], Riley Fotis[1#], Zehui Xia[2#], Kyril Kavetsky[1,3], Yung-Chien Chou[1], David Niedzwiecki[2], Michele Bondi[4], Federico Thei[4], Marija Drndić[1]*

[1]*Department of Physics and Astronomy, University of Pennsylvania, Philadelphia, PA 19104, USA*

[2]*Goeppert LLC, Philadelphia, PA 19146, USA*

[3]*Department of Material Science, University of Pennsylvania, Philadelphia, PA 19104, USA*

[4]*Elements SRL, Italy*

: these authors contribute equally
*: corresponding author
email: drndic@physics.upenn.edu

KEYWORD

Nanopore, low noise amplifier, ultrafast DNA translocation, high bandwidth

ABSTRACT

Ultrathin nanopore sensors allow single molecule and polymer measurements at sub-microsecond time resolution enabled by high current signals (~10-30 nA). We demonstrate for the first time the experimental probing of the ultrafast translocation and folding dynamics of double stranded DNA (dsDNA) through a nanopore at 10 MHz bandwidth with acquisition of data points per 25 nanoseconds (150 MB/s). By introducing a rigorous algorithm, we are able to accurately identify each current level present within translocation events and elucidate the dynamic folding and unfolding behaviors. Remarkable sensitivity of this system reveals distortions of short-lived folding states at a lower bandwidth. This work revisits probing of dsDNA as a model polymer and develops broadly applicable methods. The combined improvements in sensor signals, instrumentation and large data analysis methods uncover biomolecular dynamics at unprecedentedly small timescales.

MAIN TEXT

Nanopores allow the exploration of ion and molecular flows in constrained volumes[1, 2] and have been used to study ion transport down to atomic scales.[3] Their applications include sensors and sequencers,[4-6] filtering systems and ion-selective membranes.[2, 3, 7] More than twenty years ago solid-state nanopores were coined as new types of "microscopes" for investigating folding of polymers and probing changes in their shapes and function.[8, 9] However, experimental resolution limits still constrain fundamental insights. For example, translocations time and current distributions in low bandwidth measurements are distorted towards longer times and smaller currents.[10, 11]

Increasing accuracy requires expanding spatial-temporal resolution. Ionic currents through nanopores are typically measured at 20-500 kHz bandwidths, limiting the speed, time resolution and molecule sizes detected. Efforts have been applied on slowing down molecules[1, 2, 12-14] while small molecule detection was limited by insufficient temporal resolution.[15] Ultrafast measurements are also impeded due to sub-nA signals.[2] Recently, 1 MHz setups[16-18] provided new insights into protein folding,[19, 20] biomarker assays[21] and reducing DNA's conformational variance.[22] In addition, molecular data storage and readout applications can benefit from ultrahigh

speeds[23-25]. To further increase bandwidth[10, 26] and signal-to-noise ratio (SNR) for ultrafast analysis[26-28], low-noise nanopore chips are necessary[27].

In this Letter, we present a compact setup for the highest-bandwidth measurements, establish the upper bounds on nanopore sizes for polymer readings at 10 MHz bandwidth, and analyze double-stranded DNA (dsDNA) translocation dynamics and folding. By decreasing pore diameter from ≈ 15 nm to < 4 nm, thickness from ≈ 20 to < 5 nm, and maximizing SNR, dsDNA detection becomes possible at 10 MHz. We achieve ultralow rms noise levels at 10 MHz and record dsDNA with unprecedented accuracy at time scales < 0.1-1 μs with SNR > 4 (SNR= $\Delta \mathbf{I}/\mathbf{I}_{\mathbf{rms}}$). We perform ultrafast probing of dsDNA translocation and folding dynamics, address large dataset analysis and the important questions of signal distortions from unfolded and folded conformations due to measurement bandwidths and experimental artifacts.

Figure 1 shows the setup schematics illustrating dsDNA translocation through a nanopore of diameter *d* and thickness *t* (**Figure 1a**), 10 MHz amplifier (**Figure 1b**), transmission electron microscope (TEM) images of nanopores with thickness *t* = 20 nm and *t* = 5 nm (**Figure 1c**), the measured ionic current noise at 10 MHz bandwidth with silicon and glass chips (**Figure 1d**), and the corresponding noise power spectral density (**Figure 1e**). The portable 10 MHz setup developed by Elements srl here includes a new amplifier, allowing for a ±100 nA current range (gain 10 MΩ), voltage up to ± 1.6 V and 40 MHz sampling frequency. To make the noise as low as possible, a custom-designed flow cell with PMMA gaskets was used (**Figure S3**). A separate setup for fast pulse detection was also built to demonstrate the capability of the amplifier to detect 90 ns pulses (**Figure S4**). The measured background current and its corresponding rms noise I_{rms} *vs*. time using Si and glass chips (**Figure 1c**) are displayed in **Figure 1d** (V = 0 V, 1 M KCl at 10 MHz bandwidth). The calculated I_{rms} from Si and glass chips are 3.1 nA and 1.1 nA for these two specific chips, respectively. **Figure 1e** shows the typical noise power spectral density *vs*. frequency from both types of chips, shown in **Figure 1e** as blue and grey traces, as well as for the measured amplifier's open headstage noise (orange). At frequencies > 10^4 Hz the dominant noise is capacitive and the glass chip produces less noise than the Si chip because of its lower capacitance by at least one order of magnitude,[10, 18, 27] for the same membrane size. In the low frequency regime, the 1/f noise behavior[11, 18, 29-31] can randomly vary among pores of the same material depending on pore conditions. In fact, we can find pairwise comparisons where pores on either the

Si or the glass chip are less noisy at low bandwidth, but the high frequency range behavior is unambiguously in favor of glass chips. Noise spectra for other independent glass chips were provided in **Figure S5**. The highly reduced capacitance provided by glass reduces the noise power by a factor of 2.8 in this work at the full 10 MHz bandwidth.[26]

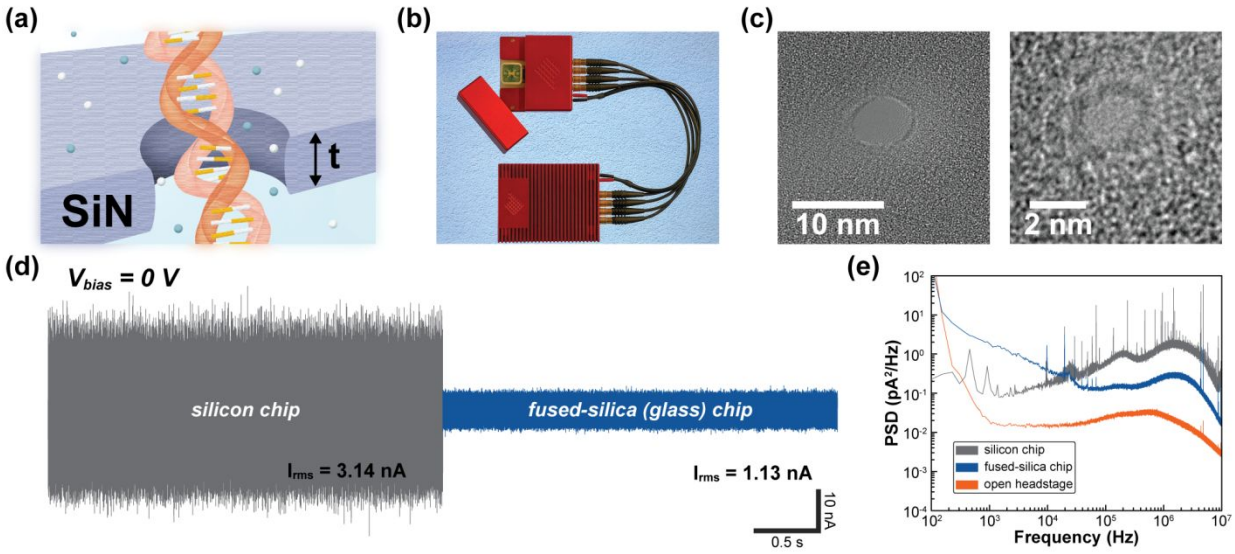

Figure 1. Experimental setup and noise performance of specific Si and glass chips. (a, b) Schematic of DNA translocation through a SiN nanopore with a new portable 10 MHz bandwidth amplifier. (c) TEM images of nanopores made in different SiN membranes on fused-silica (glass) chips. Left: ≈ 6 nm in diameter and ≈ 20 nm in thickness; right: ≈ 2.5 nm in diameter and ≈ 5 nm in thickness. (d) Baseline current traces recording at 0 mV in 1 M KCl for specific Si (left) and glass (right) chips. Corresponding baseline noise I_{rms} values are 3.14 nA and 1.13 nA for these Si and glass chips, respectively. (e) Power spectral density (PSD) analysis for the open-headstage configuration of the amplifier (orange), glass chip (blue), and Si chip (grey).

Figures 2 and **3** show experimental results that validate the pore size estimates. We show examples of 1) *negative detection results* for SiN pores with typical thickness and 1 M KCl, and 2) *positive detection results* with ultrathin pores and optimized conditions to increase the signal (3 M KCl and ~ 1V). Nanopores were drilled in JEOL F200 or JEOL 2010F TEMs with an acceleration voltage of 200 kV, and chips were inserted into a fluidic cell filled with Tris-buffered KCl solution at pH 8.

Figure 2a shows ionic current measurements at 10 MHz from a d = 15 nm nanopore in 20-nm-thick SiN. The nanopore diameter was estimated from the open pore conductance.[32] **Figure**

2a shows a ~2-s-long current trace at 300 mV when dsDNA was added in 1 M KCl. Despite adding DNA, the current *vs*. time trace is flat, similar to that without DNA, and translocation events are not observable. When this trace is filtered down to 100 kHz, translocation events distinctly emerge above the smaller noise floor and single dsDNA molecules are detected. Current blockades are ΔI ~ 0.5 - 2 nA > I_{rms} ~ 52 pA at 100 kHz (**Figure 2b**). Furthermore, the presence of two-step events indicates DNA folding.

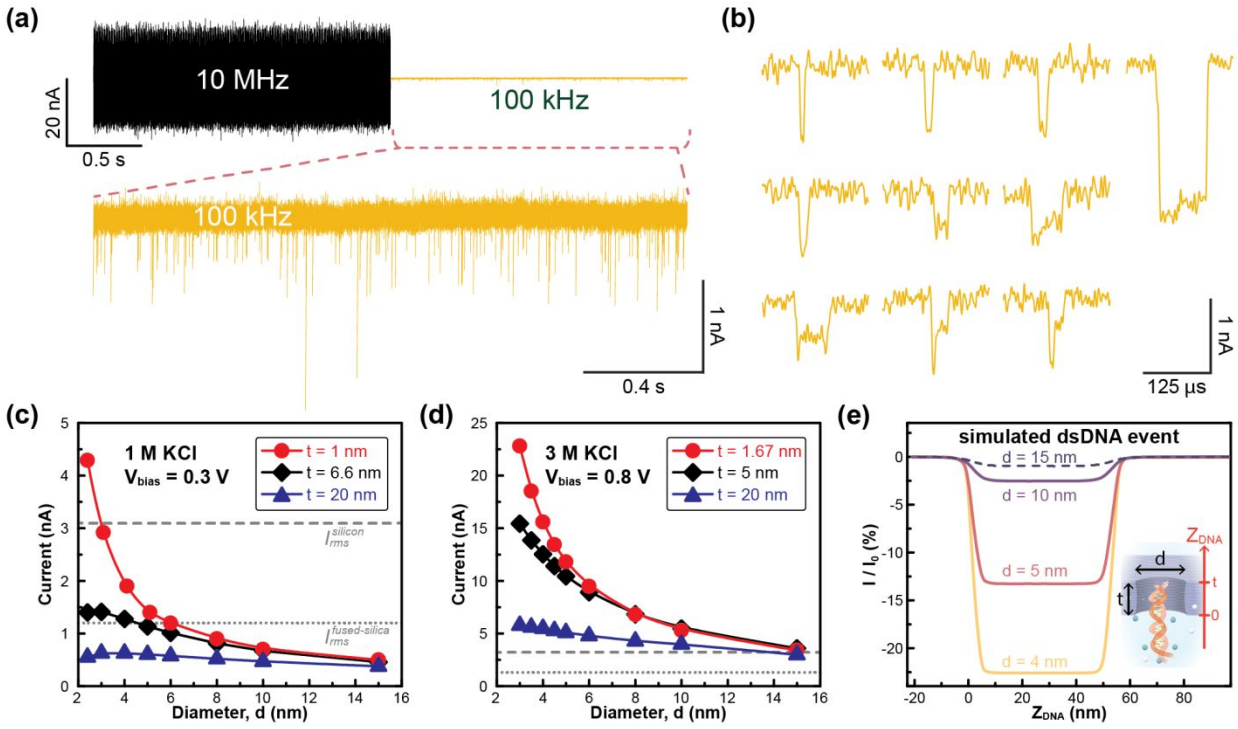

Figure 2. Emergence of dsDNA translocation events above the noise level at a lower cutoff frequency 100 kHz and corresponding simulations. (a) The 10 MHz bandwidth current vs. time trace from a 2-second-long recording obtained from 5 kbp dsDNA through a nanopore having ≈ 15 nm in diameter and ≈ 20 nm in thickness at 1M KCl and 0.3 V. Right section corresponds to the same trace filtered down to a cutoff frequency of 100 kHz, which is also magnified below. (b) Examples of translocation events from data filtered at 100 kHz. (c, d) Calculated current change, ΔI, as a function of pore diameter, *d*, for various membrane thicknesses, *t*, at different conditions. (c) 1 M KCl and 0.3 V; (d) 3 M KCl and 0.8 V. (e) Simulated blockage percentage from a 50-nm-long DNA in nanopores having various pore diameters at 3 M KCl and 0.8 V. Membrane thickness is fixed (*t* = 5 nm). Z_{DNA} denotes the z-coordinate of the DNA front.

Therefore, a larger SNR is essential in order to directly observe events at 10 MHz. This can be achieved by decreasing *d* and *t*, and increasing ion concentration and/or voltage. To quantify

this, a series of numerical simulations were conducted to examine the DNA current blockade with varying *d*, *t*, voltage and salt concentrations. The modified-Poisson-Nernst-Planck and Navier-Stokes equations were coupled to explicitly take the finite ion size and electroosmotic flow into consideration.[33, 34] Similar to conditions in **Figure 2a** (1 M KCl and 0.3 V), the maximum dsDNA current blockade ΔI *vs. d* is shown for t = 1, 6.6, and 20 nm (**Figure 2c**); t = 6.6 nm represents the effective pore thickness, about one-third of the membrane thickness for TEM-drilled pores [35]; t = 1 nm is representative of single to few-atom-thin membranes such as graphene, MoS_2, boron nitride as well as ultrathin pores in amorphous Si and SiN.[17, 26, 35-38] The dashed lines at 3.1 nA and 1.1 nA indicate experimentally extracted I_{rms} from the open pore currents at 0 V with silicon and glass chips, respectively. Another measurement is shown in **Figure 3** (I_{rms} = 1.2 nA, V = 0.8 V). The noise is reduced ≈ 2 times compared to previously published,[26] increasing SNR and sensitivity. dsDNA translocation events at 10 MHz will be undetectable using Si chips for t = 6.6 nm and 20 nm. Events are theoretically detectible with ultrathin pores (t = 1 nm) and d < 3 nm (V = 0.3 V, 1 M KCl). Using the same membrane suspended on glass, detection is possible with t = 1 nm and d < 5 nm (ΔI > 1.1 nA). The above discussion considers SNR (@10 MHz) = ΔI / I_{rms} = 1 at a V = 0.3 V in 1 M KCl. If a higher SNR is required (e.g., SNR > 4 and ΔI > 4.4 nA), events are not detectable even if t = 1 nm and d = 2.5 nm.

Larger SNRs require not only smaller and thinner pores but higher ionic concentrations and voltages. Simulations were conducted with 3 M KCl and 0.8 V accordingly. **Figure 2d** outlines possible outcomes by identifying blockade signals higher than the experimentally measured noise. For example, to achieve SNR > 5 (*i.e.*, ΔI ≥ 5.5 nA), a pore on a glass chip would need d < 8 nm, assuming t = 1.67 and 5 nm. Event depth can theoretically reach 23 nA with ultrasmall pores (t = 1.67 nm and d = 3 nm). In addition, we simulated the relative blockade percentage, ΔI/I, by varying the position of the DNA front (**Figures 2e and S7**). ΔI/I increases with decreasing d and exceeds 20% when d = 4 nm (**Figures 2e** and **S**7).

Figure 3 demonstrates *positive 10 MHz detection*, featuring dsDNA measurements with ≈ 4 times thinner (t = 5nm) pore with a ≈ 3 times smaller diameter, d ≈ 2.5 nm, measured by TEM. This pore was drilled in the locally-thinned SiN membrane on a glass chip (**Figure S1, S2**). Pore fabrication[17, 35, 39] includes electron beam lithography to pattern a 100-nm-large area, followed by reactive ion etching (RIE) for ~ 15 seconds to thin the membrane. In **Figure 3**, the pore diameter

expanded to 4.5 nm after piranha treatment (open pore conductance G ≈ 97 nS in 3 M KCl). We detected a large number of events at 300, 500 and 800 mV. The current was stable during several ≈ 10-min-long measurements and V = 800 mV was the highest voltage applied before the open pore current exceeded the current range of the amplifier (100 nA). These ultrathin pores have been tested up to 1 V over several minutes,[26] which they can withstand. Data analysis was carried out with Clampfit 10.7 and customized MATLAB code (**Supporting Information**).

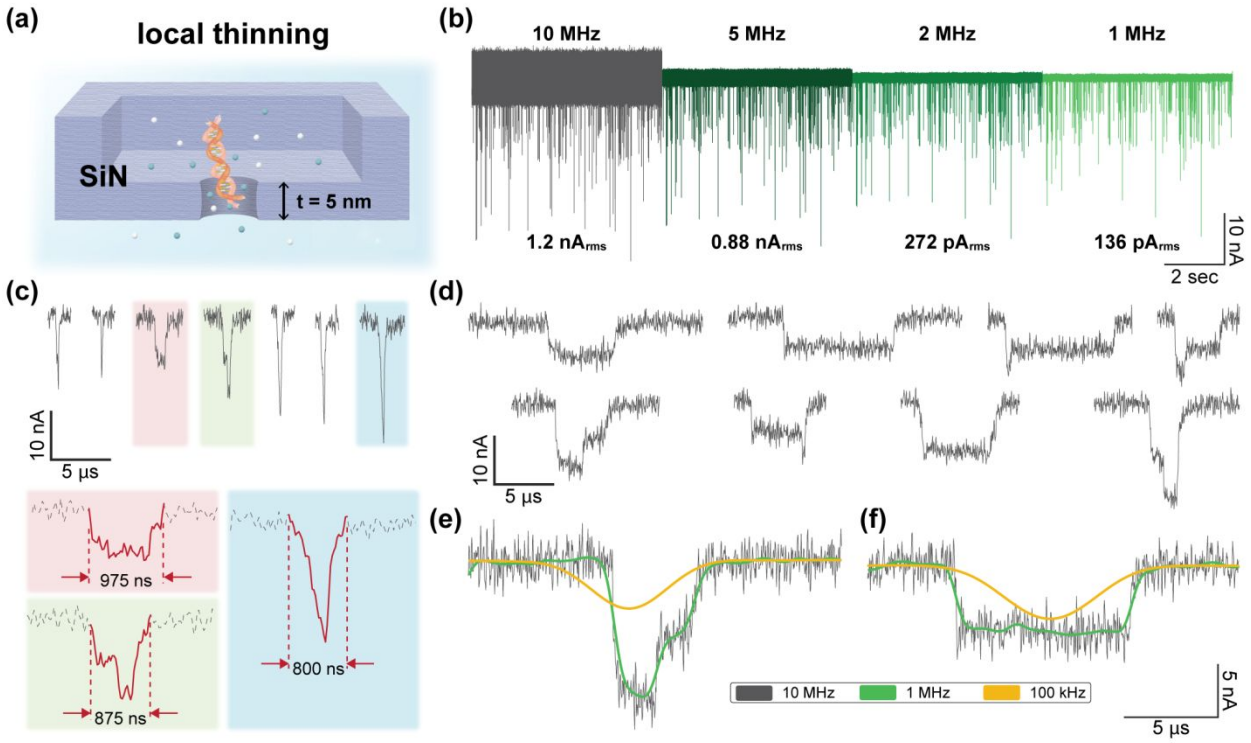

Figure 3. Event signal variation at a 10 MHz bandwidth and filtering effect. (a) Schematic illustration of dsDNA translocation through a nanopore in a locally-thinned SiN membrane on a glass chip. (b) Concatenated current trace from a 6.4-second-long recording at 800 mV and 3 M KCl. The trace exhibits visible events at a 10 MHz bandwidth (unfiltered) and is filtered using an 8-pole Bessel filter to cutoff frequencies of 5 MHz, 1 MHz, and 100 kHz. All data were recorded at 40 Msps (millions of samples per second). (c, d) Example events from 3 kbp dsDNA translocation through a ≈ 4.5-nm-diameter pore at 800 mV in 3 M KCl displaying short duration, (c), and multiple states, (d). (e) Event shape transformation and evolution during filtering: comparison of the unfiltered signal and the same signal filtered down to lower cutoff frequencies (1 MHz, green; 100 kHz, yellow). Low cutoff frequencies show progressively larger degradation of signal amplitudes and durations, especially at 100 kHz.

Table 1. Categories of one-, two-, and multiple-step events recorded at 10 MHz for applied voltage V = 800 mV in 3M KCl over 15 minutes.

	***SNR* = 4**		***SNR* = 5**	
	counts	%	counts	%
One-step	16343	49.8	5151	24.8
Two-step	12077	36.8	12552	60.5
Multiple-step	4408	13.4	3048	14.7
Total	32828	100	20751	100

Figure 3b shows a ≈ 6.4-second-long excerpt from the 15-min-long trace at V = 800 mV, displayed as 10 MHz unfiltered data with clearly visible events and the same trace filtered using an eight-pole Bessel filter to 5, 1, and 0.1 MHz; I_{rms} = 1.2 nA_{rms}, 0.88 nA_{rms}, 272 pA_{rms} and 136 pA_{rms} for 10 MHz, 5 MHz, 1 MHz, and 100 kHz, respectively. **Figure 3d** features sample events from unfiltered 10 MHz data illustrating detection of single-file (unfolded) and folded conformations of dsDNA molecules. These types of event shapes and DNA conformations in SiN pores have been well documented for dsDNA[9, 40] and studied in detail.[41] The typical one-step event is regarded as either a fully folding or unfolding event (depending on the event depth) and the two-step event as partially folding and unfolding event. Here, detection is ~ 100 times faster at 10 MHz bandwidth. These improvements allow us to observe folded, unfolded, and intermediate DNA states, with time resolution of 25 ns. As seen in **Figure 3d**, the first step in two-step events and the current change (signal sloping down) can be < 2 μs. **Figure 3c** demonstrates ultrashort signals < 1 μs. These sharp events could be translocations of DNA fragments[42] or collisions with the pore, when DNA does not overcome the energy barrier to translocate and skims the pore entrance.[43, 44]

To demonstrate insights from improved resolution, we contrast raw and filtered data to 1 MHz and 100 kHz (**Figures 3e,f and S8**). For events shorter than 10 μs, filtering to 100 kHz introduces significant distortions: (i) the features of two-step and multiple-step events disappear (**Figures 3e and S8a,b**), (ii) event depths are attenuated by 10-50% (**Table S1**), and (iii) the dwell times are ≈ 2 times longer (**Table S1**). For one-step events (**Figure 3f**), the dwell time is 1.5 times longer. The

folded feature vanishes as well for events > 10 μs if small portion of DNA is folded (**Figure S8c**). For multiple-step events > 10 μs, event shapes distort as bandwidth decreases and information is lost. For example, in the 17.5 μs-long event (**Figure S8d)**, fine signal features are lost.

Improved time resolution and smaller current distortions are attained using 10 MHz bandwidth. Below we quantify these two aspects and show the improved insights into the dsDNA translocation and folding dynamics. First, in order to analyze such large datasets improved algorithms were needed. To this end, we developed a customized MATLAB code to detect events and categorize them by number of internal steps, defined by sudden current changes (see **Figure 4a** and **Supporting Information 4.3** for details). Events were categorized into one-, two-, and multiple-step events; ≈ 49% of events were one-step and ≈ 37% of events two-step (**Table 1**) with SNR = 4 as the detection threshold. Two-step events became dominant (60%) as SNR increased to 5. The large numbers of detected events within 15 min were n = 32828 and n = 20751 for SNR = 4 and SNR = 5, respectively. Two-step events were either "step-up" or "step-down", as defined in **Figure 4b**, and step-up events dominated (> 73%).

One-step events have three possible mean depths represented by peak depths 7.1, 11.8, and 23.7 nA, corresponding to unfolded and folded dsDNA (**Figure 4b (i)**). We perform a finer analysis of two-step events by carrying out separate analyses of step-up and step-down events. We label the first (1) and second (2) steps as $S_{1u,d}$ and $S_{2u.d}$, respectively, and $\Delta I_{1u,d}$ ($\Delta I_{2u,d}$) and $\tau_{1u,d}$ ($\tau_{2u,d}$) as the depths and dwell times for step-up and step-down event distributions **(Figure 4b (ii)** and **(iii)**); subscript "u" refers to step-up and "d" to step-down events. For step-up events, two well-separated peaks are observed with the peak depths 11.7 (S_{1u}) and 6.6 nA (S_{2u}), which line up well with the first two populations in the one-step event distribution. This strongly suggests that step-up events correspond to translocations of folded DNA chains entering the pore, followed by unfolded parts.[9, 32, 40] In contrast, for step-down events (**Figure 4b (iii)**), steps S_{1d} and S_{2d} are closer to each other and a third peak is observed at ~24.4 nA from S_{2d}. Peak values for S_{1d} and S_{2d} (5.1 and 6.9 nA, respectively) do not match the corresponding peaks in one-step and step-up events, and are both shifted to lower ΔI. A majority of step-down events contain shallower first steps ($\Delta I_{2d}/\Delta I_{1d} < 2$) that have been attributed previously to DNA blocking the access region or being trapped at the pore entrance.[10, 16, 36, 45]

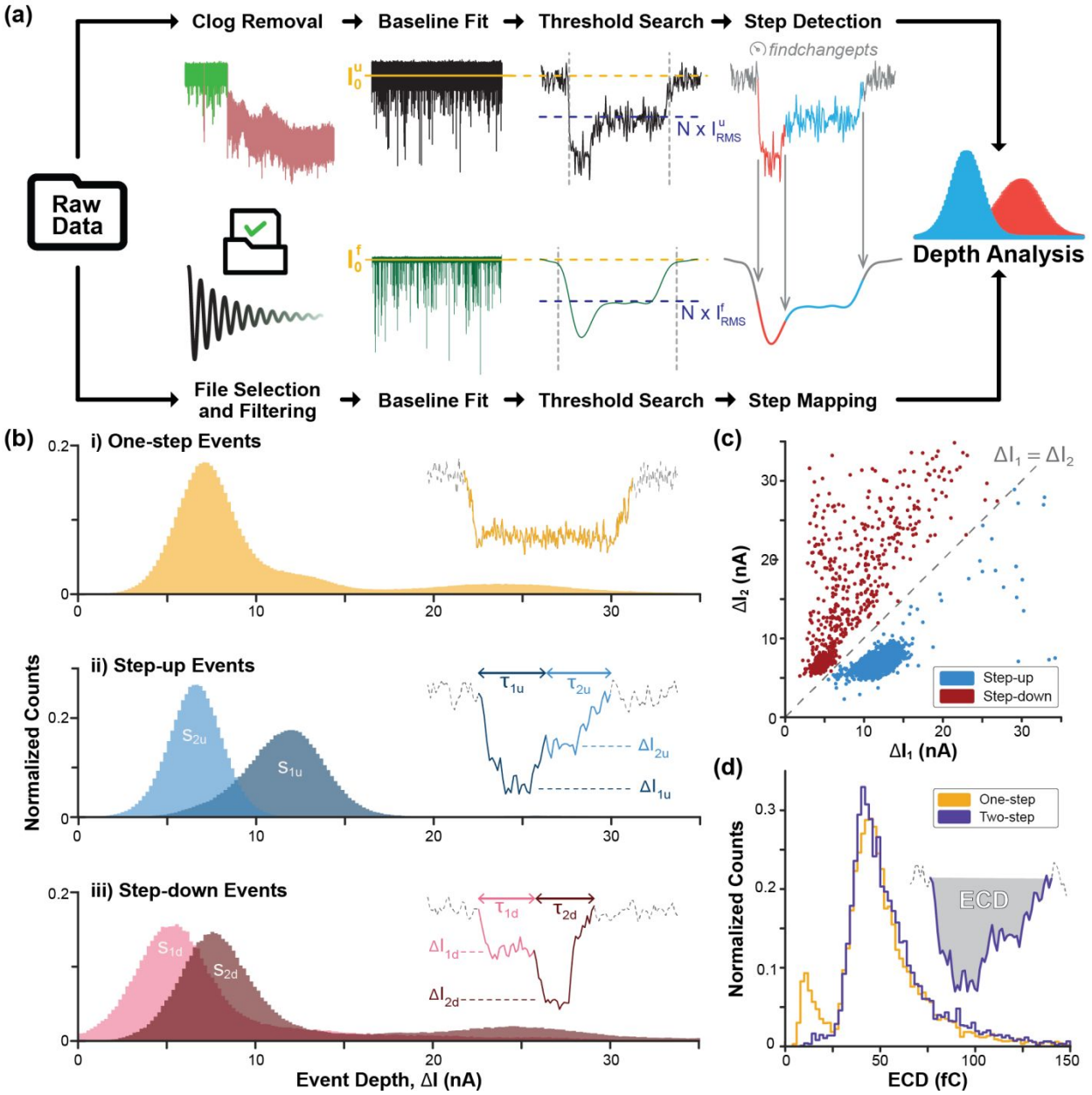

Figure 4. **Translocation event statistics.** (a) Flow chart detailing the data analysis process. Here I_0^u and I_0^f are the unfiltered and filtered baseline currents, respectively; I_{RMS}^u and I_{RMS}^f are the I_{rms} obtained from unfiltered and filtered data, respectively. N is the degree of SNR. (b) Histogram plot of event counts *vs.* event depth for one-step and two-step events. S_1 and S_2 (with subscripts u for step-up and d for step-down) represent the first and second steps of the two-step events, respectively. The label "Step-up" ("Step-down") event is used to denote that a deeper level occurs before (after) the shallower level. (c) Mean current blockage scatter plot, ΔI_1 *vs.* ΔI_2, for two-step event data presented in (a). ΔI_1 (ΔI_2) is defined as the event depth for the first (second) subevent in two-step events. Dashed-line denotes a boundary at $\Delta I_1 = \Delta I_2$. (d) Histograms of ECD for one-step events (n = 17216), and two-step events (n = 11074). Similar ECD distributions imply that collected events originate from the DNA of the same length.

The event depths for each step in the two-step events, ΔI_2 *vs.* ΔI_1, are plotted in **Figure 4c**, displaying two clouds representative of step-up (blue) and step-down (red) events. A localized distribution in the range of 5 to 15 nA is observed for step-up events, whereas a wider spread in ΔI is shown for step-down events. Electrical charge deficit (ECD), which is the integral of current blockage over the duration of an event (illustrated in **Figure 4d**), is useful in resolving multiple states of dsDNA such as folded and unfolded configurations.[44, 46] **Figure 4d** shows that, with ECD > 25 fC, ECD distribution having a peak of ≈ 40 fC is remarkably similar for one-step and two-step events, suggesting that collected events are indeed from the same DNA length. For one-step events, a single peak at a low ECD value (≈ 12 fC) is observed. These events could be translocations of DNA fragments[42, 44] or collisions with pore entrance[43] (**Figure 3c**).

The insights obtained from the first step within step-up events are particularly relevant to the folding state during the translocation. We show how the folding state dynamics and the short timescales are captured more accurately with 10 MHz data, in contrast to filtered data at 1 MHz. **Figure 5a** shows the distribution of durations, $\tau_{1u,}$, of the first steps in the two-step events and an exponential fit with the characteristic timescale of $\tau_{1u} \sim 1.66$ μs. The relatively short durations raise an important question: how does the filtering distort the signal of folded states? We compare the event depth of the first step in step-up events (*i.e.*, ΔI_{1u}) between 10 MHz raw data and 1 MHz filtered data (**Figure 5b**). Three different regimes are examined: $\tau_{1u} < 1$ μs, 1 μs < $\tau_{1u} < 2$ μs, and $\tau_{1u} > 2$ μs. The peak values for ΔI_{1u} for unfiltered 10 MHz and 1 MHz filtered data align when τ_{1u} > 2 μs. However, if $\tau_{1u} < 2$ μs, distributions of 1 MHz filtered data shift to a lower ΔI_{1u}. The difference between unfiltered 10 MHz and 1 MHz filtered data is significant when $\tau_{1u} < 1$ μs. This discrepancy indicates the magnitude of attenuation in the 1 MHz filtered data.

To quantify the current attenuation due to filtering, the difference between unfiltered and filtered ΔI_{1u} is shown in **Figure 5c**. We define the "percentage current agreement" $PCA = 1 - (\Delta I_{1u} - \Delta I_{1u,filtered})/(\Delta I_{1u} - \Delta I_{2u})$, where subscript "filtered" denotes results from filtered data; *PCA* can range from 0, corresponding to no agreement and complete attenuation of the filtered signal, to 1, for complete agreement and no attenuation of the filtered signal. The experimental results (black symbols) agree well with the simulated agreement (red curve) which is based on ideal pulses (see **Supporting Information 4.4**). **Figure 5c** clearly shows that attenuation becomes increasingly significant with decreasing τ_{1u}. For $\tau_{1u} = 0.625$ to 0.75 μs, ΔI_1 is attenuated by up to 50% in the

filtered step. We also show that ECD is not a reliable tool for identifying the attenuation and distortion of events due to low bandwidth (**Figure S12**). The 10 MHz data more accurately captures the folding dynamics at unprecedented timescales. Results in **Figure 5** show the importance of time resolution on elucidating dsDNA configuration.

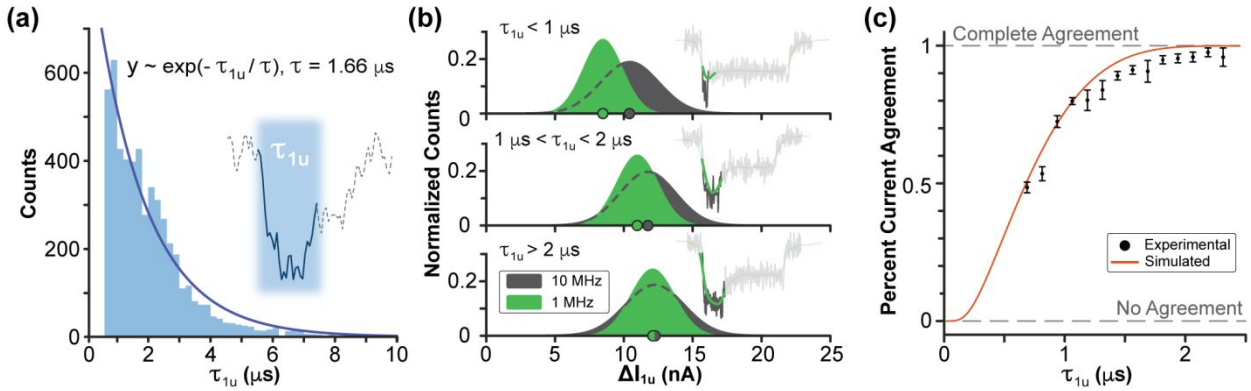

Figure 5. **Distribution and distortion of τ_{1u}.** (a) Histogram of τ_{1u} from the "step-up" events presented in Figure 4a. (b) Histogram plot of counts *vs.* ΔI_{1u} for 10 MHz unfiltered and 1 MHz filtered data by varying three regimes of τ_{1u}. The discrepancy is largest for $\tau_{1u} < 1$ μs. (c) Variation of percent current attenuation (PCA) with τ_{1u} for Figure 5b. Red curve is obtained by simulating an ideal pulse having two steps (see Supporting Information).

In summary, the dynamic folding and unfolding behaviors of DNA have been investigated thoroughly at 10 MHz bandwidth (~100 ns time resolution) by using the low noise chips. Our results demonstrate that, to achieve acceptable signal-to-noise ratios, pores should be smaller and thinner (~ sub-5 nm) with high voltages and salt concentrations, as supported by our theoretical model. High temporal resolution of this system not only detects ultrafast DNA translocations but also captures features that occur within extremely short duration. We presented a rigorous algorithm to detect the translocation events and analyze event features. The distributions of each current level in two-step events provide more accurate data of unfolded and folded configurations as well as the interactions between pores and DNA. We also exploit step-up events, which correspond to partially folded DNA configurations, to probe the dynamics of the folding state during translocation, thereby quantifying the attenuations of event depth within short durations. Our results demonstrate a versatile platform able to investigate single molecule events lasting less than hundreds of nanoseconds, allowing accurate ultrafast DNA translocation measurements.

ASSOCIATED CONTENT

NOTES

The authors declare the following potential competing financial interest(s): M.D. is a founder and consultant of Goeppert (*www.gppert.com*) that manufactures nanopore chips, fluid cells, and TEM supplies.

Supporting Information.

Additional information on the measurement electronics, nanopore fabrication, data analysis, and two-level event structure in the translocation experiments is found in the Supplementary Information. This material is available free of charge via the Internet at http://pubs.acs.org.

AUTHOR INFORMATION

Corresponding Author

*Email: drndic@physics.upenn.edu

ACKNOWLEDGMENT

This work was partially funded by NSF grants 2002477, 190504, NIH grant R21 HG0101536 at the University of Pennsylvania, and NASA Small Business Technology Transfer (STTR) Award 80NSSC21C0368 at Goeppert LLC. Work by M.B. and F.T. at Elements SRL was partially supported by the University of Pennsylvania, Prof. M.D. We acknowledge the use of the JEOL F200 TEM at the University of Pennsylvania and JEOL 2010F TEM at Rutgers University for nanopore fabrication and imaging (Figure 2). This work was partially performed at the Singh Center for Nanotechnology, an NNCI member supported by NSF Grant NNCI-2025608. We thank Andre Scott from Goeppert LLC for fabricating glass chips. C.-Y.L. is grateful to Dr. Douglas Yates for TEM assistance and Chen Lo for graphic design. C.-Y.L., Z.X. and M.D. conceived the experiments. C.-Y.L, Z.X., and Y.-C. C. setup 10 MHz measurements and performed TEM imaging. R.F., K.K. and C.-Y.L. developed data analysis protocols and analyzed current traces. Z.X. and D.N. contributed to thin glass chip design. M.B. and F.T. designed the circuitry, built and tested the portable 10 MHz amplifier. C.-Y.L. carried out the finite element analysis (COMSOL) modeling. All authors discussed the manuscript and contributed throughout the writing process.

REFERENCE

(1) Branton, D.; Deamer, D. W.; Marziali, A.; Bayley, H.; Benner, S. A.; Butler, T.; Di Ventra, M.; Garaj, S.; Hibbs, A.; Huang, X. H.; et al. The potential and challenges of nanopore sequencing. *Nat. Biotechnol.* **2008**, *26* (10), 1146-1153. DOI: 10.1038/nbt.1495.
(2) Xue, L.; Yamazaki, H.; Ren, R.; Wanunu, M.; Ivanov, A. P.; Edel, J. B. Solid-state nanopore sensors. *Nat. Rev. Mater.* **2020**, *5* (12), 931-951. DOI: 10.1038/s41578-020-0229-6.
(3) Thiruraman, J. P.; Masih Das, P.; Drndić, M. Ions and Water Dancing through Atom-Scale Holes: A Perspective toward "Size Zero". *ACS Nano* **2020**, *14* (4), 3736-3746. DOI: 10.1021/acsnano.0c01625.
(4) Noakes, M. T.; Brinkerhoff, H.; Laszlo, A. H.; Derrington, I. M.; Langford, K. W.; Mount, J. W.; Bowman, J. L.; Baker, K. S.; Doering, K. M.; Tickman, B. I.; et al. Increasing the accuracy of nanopore DNA sequencing using a time-varying cross membrane voltage. *Nat. Biotechnol.* **2019**, *37* (6), 651-656. DOI: 10.1038/s41587-019-0096-0.
(5) Laszlo, A. H.; Derrington, I. M.; Ross, B. C.; Brinkerhoff, H.; Adey, A.; Nova, I. C.; Craig, J. M.; Langford, K. W.; Samson, J. M.; Daza, R.; et al. Decoding long nanopore sequencing reads of natural DNA. *Nat. Biotechnol.* **2014**, *32* (8), 829-833. DOI: 10.1038/nbt.2950.
(6) Jain, M.; Koren, S.; Miga, K. H.; Quick, J.; Rand, A. C.; Sasani, T. A.; Tyson, J. R.; Beggs, A. D.; Dilthey, A. T.; Fiddes, I. T.; et al. Nanopore sequencing and assembly of a human genome with ultra-long reads. *Nat. Biotechnol.* **2018**, *36* (4), 338-345. DOI: 10.1038/nbt.4060.
(7) Danda, G.; Drndić, M. Two-dimensional nanopores and nanoporous membranes for ion and molecule transport. *Curr. Opin. Biotechnol.* **2019**, *55*, 124-133. DOI: 10.1016/j.copbio.2018.09.002.
(8) Li, J.; Stein, D.; McMullan, C.; Branton, D.; Aziz, M. J.; Golovchenko, J. A. Ion-beam sculpting at nanometre length scales. *Nature* **2001**, *412* (6843), 166-169. DOI: 10.1038/35084037.
(9) Li, J.; Gershow, M.; Stein, D.; Brandin, E.; Golovchenko, J. A. DNA molecules and configurations in a solid-state nanopore microscope. *Nat. Mater.* **2003**, *2* (9), 611-615. DOI: 10.1038/nmat965.
(10) Shekar, S.; Niedzwiecki, D. J.; Chien, C.-C.; Ong, P.; Fleischer, D. A.; Lin, J.; Rosenstein, J. K.; Drndić, M.; Shepard, K. L. Measurement of DNA Translocation Dynamics in a Solid-State Nanopore at 100 ns Temporal Resolution. *Nano Lett.* **2016**, *16* (7), 4483-4489. DOI: 10.1021/acs.nanolett.6b01661.
(11) Uram, J. D.; Ke, K.; Mayer, M. Noise and Bandwidth of Current Recordings from Submicrometer Pores and Nanopores. *ACS Nano* **2008**, *2* (5), 857-872. DOI: 10.1021/nn700322m.
(12) Kowalczyk, S. W.; Wells, D. B.; Aksimentiev, A.; Dekker, C. Slowing down DNA Translocation through a Nanopore in Lithium Chloride. *Nano Lett.* **2012**, *12* (2), 1038-1044. DOI: 10.1021/nl204273h.
(13) Mirsaidov, U.; Comer, J.; Dimitrov, V.; Aksimentiev, A.; Timp, G. Slowing the translocation of double-stranded DNA using a nanopore smaller than the double helix. *Nanotechnology* **2010**, *21* (39), 395501. DOI: 10.1088/0957-4484/21/39/395501.
(14) Deamer, D.; Akeson, M.; Branton, D. Three decades of nanopore sequencing. *Nat. Biotechnol.* **2016**, *34* (5), 518-524. DOI: 10.1038/nbt.3423.
(15) Plesa, C.; Kowalczyk, S. W.; Zinsmeester, R.; Grosberg, A. Y.; Rabin, Y.; Dekker, C. Fast Translocation of Proteins through Solid State Nanopores. *Nano Lett.* **2013**, *13* (2), 658-663. DOI: 10.1021/nl3042678.

(16) Rosenstein, J. K.; Wanunu, M.; Merchant, C. A.; Drndic, M.; Shepard, K. L. Integrated nanopore sensing platform with sub-microsecond temporal resolution. *Nat. Methods.* **2012**, *9* (5), 487-492. DOI: 10.1038/nmeth.1932.
(17) Venta, K.; Shemer, G.; Puster, M.; Rodríguez-Manzo, J. A.; Balan, A.; Rosenstein, J. K.; Shepard, K.; Drndić, M. Differentiation of Short, Single-Stranded DNA Homopolymers in Solid-State Nanopores. *ACS Nano* **2013**, *7* (5), 4629-4636. DOI: 10.1021/nn4014388.
(18) Balan, A.; Machielse, B.; Niedzwiecki, D.; Lin, J.; Ong, P.; Engelke, R.; Shepard, K. L.; Drndić, M. Improving Signal-to-Noise Performance for DNA Translocation in Solid-State Nanopores at MHz Bandwidths. *Nano Lett.* **2014**, *14* (12), 7215-7220. DOI: 10.1021/nl504345y.
(19) Larkin, J.; Henley, R. Y.; Muthukumar, M.; Rosenstein, Jacob K.; Wanunu, M. High-Bandwidth Protein Analysis Using Solid-State Nanopores. *Biophys. J.* **2014**, *106* (3), 696-704. DOI: 10.1016/j.bpj.2013.12.025.
(20) Tripathi, P.; Firouzbakht, A.; Gruebele, M.; Wanunu, M. Direct Observation of Single-Protein Transition State Passage by Nanopore Ionic Current Jumps. *J. Phys. Chem. Lett.* **2022**, *13* (25), 5918-5924. DOI: 10.1021/acs.jpclett.2c01009.
(21) He, L.; Tessier, D. R.; Briggs, K.; Tsangaris, M.; Charron, M.; McConnell, E. M.; Lomovtsev, D.; Tabard-Cossa, V. Digital immunoassay for biomarker concentration quantification using solid-state nanopores. *Nat. Commun.* **2021**, *12* (1), 5348. DOI: 10.1038/s41467-021-25566-8.
(22) Briggs, K.; Madejski, G.; Magill, M.; Kastritis, K.; de Haan, H. W.; McGrath, J. L.; Tabard-Cossa, V. DNA Translocations through Nanopores under Nanoscale Preconfinement. *Nano Lett.* **2018**, *18* (2), 660-668. DOI: 10.1021/acs.nanolett.7b03987.
(23) Chen, K.; Kong, J.; Zhu, J.; Ermann, N.; Predki, P.; Keyser, U. F. Digital Data Storage Using DNA Nanostructures and Solid-State Nanopores. *Nano Lett.* **2019**, *19* (2), 1210-1215. DOI: 10.1021/acs.nanolett.8b04715.
(24) Bošković, F.; Ohmann, A.; Keyser, U. F.; Chen, K. DNA Structural Barcode Copying and Random Access. *Small Structures* **2021**, *2* (5), 2000144. DOI: 10.1002/sstr.202000144.
(25) Chen, K.; Zhu, J.; Bošković, F.; Keyser, U. F. Nanopore-Based DNA Hard Drives for Rewritable and Secure Data Storage. *Nano Lett.* **2020**, *20* (5), 3754-3760. DOI: 10.1021/acs.nanolett.0c00755.
(26) Chien, C.-C.; Shekar, S.; Niedzwiecki, D. J.; Shepard, K. L.; Drndić, M. Single-Stranded DNA Translocation Recordings through Solid-State Nanopores on Glass Chips at 10 MHz Measurement Bandwidth. *ACS Nano* **2019**, *13* (9), 10545-10554. DOI: 10.1021/acsnano.9b04626.
(27) Balan, A.; Chien, C.-C.; Engelke, R.; Drndić, M. Suspended Solid-state Membranes on Glass Chips with Sub 1-pF Capacitance for Biomolecule Sensing Applications. *Sci. Rep.* **2015**, *5* (1), 17775. DOI: 10.1038/srep17775.
(28) Niedzwiecki, D. J.; Chou, Y.-C.; Xia, Z.; Thei, F.; Drndić, M. Detection of single analyte and environmental samples with silicon nitride nanopores: Antarctic dirt particulates and DNA in artificial seawater. *Rev. Sci. Instrum.* **2020**, *91* (3), 031301. DOI: 10.1063/1.5138210.
(29) Fragasso, A.; Pud, S.; Dekker, C. 1/f noise in solid-state nanopores is governed by access and surface regions. *Nanotechnology* **2019**, *30* (39), 395202. DOI: 10.1088/1361-6528/ab2d35.
(30) Fragasso, A.; Schmid, S.; Dekker, C. Comparing Current Noise in Biological and Solid-State Nanopores. *ACS Nano* **2020**, *14* (2), 1338-1349. DOI: 10.1021/acsnano.9b09353.
(31) Smeets, R. M. M.; Keyser, U. F.; Dekker, N. H.; Dekker, C. Noise in solid-state nanopores. *Proceedings of the National Academy of Sciences* **2008**, *105* (2), 417-421. DOI: doi:10.1073/pnas.0705349105.

(32) Chou, Y. C.; Chen, J.; Lin, C. Y.; Drndic, M. Engineering adjustable two-pore devices for parallel ion transport and DNA translocations. *J. Chem. Phys.* **2021**, *154* (10), 105102. DOI: Artn 105102
10.1063/5.0044227.
(33) Lin, C.-Y.; Turker Acar, E.; Polster, J. W.; Lin, K.; Hsu, J.-P.; Siwy, Z. S. Modulation of Charge Density and Charge Polarity of Nanopore Wall by Salt Gradient and Voltage. *ACS Nano* **2019**, *13* (9), 9868-9879. DOI: 10.1021/acsnano.9b01357.
(34) Kilic, M. S.; Bazant, M. Z.; Ajdari, A. Steric effects in the dynamics of electrolytes at large applied voltages. II. Modified Poisson-Nernst-Planck equations. *Phys. Rev. E* **2007**, *75* (2), 021503. DOI: 10.1103/PhysRevE.75.021503.
(35) Wanunu, M.; Dadosh, T.; Ray, V.; Jin, J. M.; McReynolds, L.; Drndic, M. Rapid electronic detection of probe-specific microRNAs using thin nanopore sensors. *Nat. Nanotechnol.* **2010**, *5* (11), 807-814. DOI: 10.1038/Nnano.2010.202.
(36) Rodríguez-Manzo, J. A.; Puster, M.; Nicolaï, A.; Meunier, V.; Drndić, M. DNA Translocation in Nanometer Thick Silicon Nanopores. *ACS Nano* **2015**, *9* (6), 6555-6564. DOI: 10.1021/acsnano.5b02531.
(37) Gilboa, T.; Zrehen, A.; Girsault, A.; Meller, A. Optically-Monitored Nanopore Fabrication Using a Focused Laser Beam. *Sci. Rep.* **2018**, *8* (1), 9765. DOI: 10.1038/s41598-018-28136-z.
(38) Yamazaki, H.; Hu, R.; Zhao, Q.; Wanunu, M. Photothermally Assisted Thinning of Silicon Nitride Membranes for Ultrathin Asymmetric Nanopores. *ACS Nano* **2018**, *12* (12), 12472-12481. DOI: 10.1021/acsnano.8b06805.
(39) Drndic, M.; Wanunu, M.; Dadosh, T. High-Resolution Analysis Devices and Related Methods. 2015.
(40) Storm, A. J.; Chen, J. H.; Zandbergen, H. W.; Dekker, C. Translocation of double-strand DNA through a silicon oxide nanopore. *Phys. Rev. E* **2005**, *71* (5), 051903. DOI: 10.1103/PhysRevE.71.051903.
(41) Carson, S.; Wilson, J.; Aksimentiev, A.; Wanunu, M. Smooth DNA Transport through a Narrowed Pore Geometry. *Biophys. J.* **2014**, *107* (10), 2381-2393. DOI: 10.1016/j.bpj.2014.10.017.
(42) Mihovilovic, M.; Hagerty, N.; Stein, D. Statistics of DNA Capture by a Solid-State Nanopore. *Phys. Rev. Lett.* **2013**, *110* (2), 028102. DOI: 10.1103/PhysRevLett.110.028102.
(43) Wanunu, M.; Sutin, J.; McNally, B.; Chow, A.; Meller, A. DNA Translocation Governed by Interactions with Solid-State Nanopores. *Biophys. J.* **2008**, *95* (10), 4716-4725. DOI: 10.1529/biophysj.108.140475.
(44) Bell, N. A. W.; Muthukumar, M.; Keyser, U. F. Translocation frequency of double-stranded DNA through a solid-state nanopore. *Phys. Rev. E* **2016**, *93* (2), 022401. DOI: 10.1103/PhysRevE.93.022401.
(45) Carlsen, A. T.; Zahid, O. K.; Ruzicka, J.; Taylor, E. W.; Hall, A. R. Interpreting the Conductance Blockades of DNA Translocations through Solid-State Nanopores. *ACS Nano* **2014**, *8* (5), 4754-4760. DOI: 10.1021/nn501694n.
(46) Fologea, D.; Gershow, M.; Ledden, B.; McNabb, D. S.; Golovchenko, J. A.; Li, J. Detecting Single Stranded DNA with a Solid State Nanopore. *Nano Lett.* **2005**, *5* (10), 1905-1909. DOI: 10.1021/nl051199m.

For Table of Contents Only